Title

Scalable single-mode surface-emitting laser via open-Dirac singularities

Journal

Nature, 608(7924)

ISSN

0028-0836

Authors

Contractor, Rushin
Noh, Wanwoo
Redjem, Walid
et al.

Publication Date

2022-08-25

DOI

10.1038/s41586-022-05021-4

nature

https://doi.org/10.1038/s41586-022-05021-4

Accelerated Article Preview

Scalable single-mode surface emitting laser via open-Dirac singularities

Received: 31 January 2022

Accepted: 23 June 2022

Accelerated Article Preview

Cite this article as: Contractor, R. et al. Scalable single-mode surface emitting laser via open-Dirac singularities. *Nature* https://doi.org/10.1038/s41586-022-05021-4 (2022)

Rushin Contractor, Wanwoo Noh, Walid Redjem, Wayesh Qarony, Emma Martin, Scott Dhuey, Adam Schwartzberg & Boubacar Kanté

Scalable single-mode surface emitting laser via open-Dirac singularities

Rushin Contractor[1]*, Wanwoo Noh[1]*, Walid Redjem*[1], Wayesh Qarony[2], Emma Martin[1], Scott Dhuey[3], Adam Schwartzberg[3], and Boubacar Kanté[1,2†]

[1]*Department of Electrical Engineering and Computer Sciences, University of California, Berkeley, California 94720, USA*

[2]*Materials Sciences Division, Lawrence Berkeley National Laboratory, 1 Cyclotron Road, Berkeley, California 94720, USA*

[3]*Molecular Foundry, Lawrence Berkeley National Laboratory, Berkeley, California 94720, USA*

[†]bkante@berkeley.edu

*These authors contributed equally to this work

Single-aperture cavities are a key component of lasers, instrumental for the amplification and emission of a single light mode. However, the appearance of high-order transverse modes as cavities size increases has frustrated efforts to scale up cavities whilst preserving single-mode operation since the invention of the laser six decades ago [1-8]. A suitable physical mechanism that allows single-mode lasing irrespective of the cavity size – a "scale-invariant" cavity or laser – has not been identified yet. Here, we propose and demonstrate experimentally that open-Dirac electromagnetic cavities with linear dispersion – which in our devices are realized by a truncated photonic crystal arranged in a hexagonal pattern – exhibit unconventional scaling of losses in reciprocal space, leading to single-mode lasing that is maintained as the cavity is scaled up in size. The physical origin of this phenomenon lies in the convergence of the complex part of the free spectral range in open-Dirac cavities towards a constant governed by the loss rate of distinct Bloch band, while for common cavities it converges to zero as the size grows, leading to inevitable multi-mode emission. An unconventional flat envelope fundamental mode locks all unit-cells in the cavity in phase, leading to single-mode lasing. We name such sources Berkeley Surface Emitting Lasers (BerkSELs) and demonstrate that their far-field corresponds to a topological singularity of charge two, in agreement with our theory. Open-Dirac cavities unlock new avenues for light-matter interaction and cavity quantum electrodynamics.

Dirac points are topological singularities that have attracted enormous interests since the discovery of massless Dirac fermions governing electronic transport in graphene [9]. Their occurrence usually indicates an imminent topological transition, and they are at the heart of the physics of topological insulators [10]. In general, wave systems that possess a band structure, such as photonic crystals [11-12], also exhibit Dirac cones (DCs) and it was demonstrated that DCs are universal features that can be systematically implemented by controlling the symmetry of the structure [13-14]. In photonics, DCs have mostly been utilized to demonstrate effective zero-index materials and their properties or to control the dispersion of polaritons [15-20]. Recently, a DC implemented using a three-dimensional structure was theoretically proposed to enable large area single-mode lasing [21-22]. However, the proposed mechanism relied on changes in the real part of the frequency spacing of the cavity modes that increases by an amount much smaller than the typical gain bandwidth of semiconductors and is thus insufficient to enable single-mode operation in lasers. Moreover, all observed modes exhibited oscillatory wavefunctions.

Surface emitting lasers have played a fundamental role in science and technology since the invention of lasers [1], the demonstration of distributed feedback lasers [2], as well as the invention of vertical cavity surface emitting lasers [3]. Scaling the cavity aperture has since been a challenge. We report, a room temperature scalable open-Dirac lasing cavity that exploits the linear dispersion of photons near the band edge of a photonic crystal, and that can be scaled to large sizes. Our proposed structure is presented in Fig. 1a. It is a photonic crystal (PhC) with a hexagonal lattice. The unit-cell of the PhC is presented in the inset of Fig. 1b. The linear dispersion of Fig. 1c is obtained for a laterally infinite structure (X-Y direction) by overlapping doubly degenerate modes of the E_2 irreducible representation with a singly-degenerate mode of the B_1 irreducible representation from the C_{6v} point group at the Γ-point of the Brillouin zone [13-14] (see Supplementary Information). The degeneracy of the modes is obtained for a critical radius of holes r_{Dirac}. An open-Dirac cavity, shown in Fig. 1, is formed by truncating the infinite PhC as a hexagon around a central air-hole with edges normal to the M-directions of the lattice. The entire cavity is suspended in air, and it is connected to the main membrane by six bridges at the corners of the hexagon for mechanical stability (Fig. 1a-b). The structure is fabricated using electron-beam lithography and the PhC is defined by inductively coupled plasma etching, followed by a wet etching step to create the suspended membrane (see Supplementary Information).

Three modes are involved in the formation of the Dirac cone. The coupling between the B and E modes is direction-dependent and one of the E modes forms a flat band as seen in Fig. 1c. Therefore, the interaction between the B and E modes detuned in frequency by ϵ can be expressed in a simplified form by the Hamiltonian,

$$H = \begin{pmatrix} 0 & \beta k \\ \beta k & \epsilon \end{pmatrix}, \tag{1}$$

where k is the Bloch momentum and β is a coupling constant. As $\epsilon \rightarrow 0$, the eigenfrequencies of H form bands with a linear dependence on k. Moreover, the eigenvectors of H are mixed and the orthogonal modes B and E are transformed into an admixture of B±E as we move away from $k = 0$. When a system with the interaction Hamiltonian H is truncated to a finite cavity, the linear bands break up into discrete modes. This idea is demonstrated in Fig. 2a where the dispersion of the PhC at r_{Dirac} is overlaid on the discrete cavity modes. The color of these modes indicates the purity of the eigenvector. We observe that when we are close to the Dirac singularity, only the fundamental mode at the Γ-point is purely B. Higher order modes originating from both the B and E bands consist of an admixture of fields from both these bands. The separation between modes $\delta_k \sim \pi/D$ is governed by the length of the cavity D. The finite size of the cavity also introduces an uncertainty in the momentum space σ_k. We further note that no pure E mode at the Γ-point exists due to the six-fold rotational symmetry of the cavity. The E modes only have two-fold rotational symmetry and hence a fundamental mode which is spread across the entire cavity cannot originate from the E band. The presence of the corners also eliminates feedback along the K-direction of the Brillouin zone and high-quality factor (Q) modes are supported only along the M-direction. The five lowest order modes are computed for a cavity with *D*=51a (where a is the size of the unit-cell) and presented in Fig. 2a labelled as $|0\rangle$-$|4\rangle$ with mode $|0\rangle$ being the fundamental mode.

The linear dispersion around the open-Dirac singularity means that the fundamental mode effectively sees zero refractive index. This means that, unlike the fundamental mode of conventional PhC cavities which have a Gaussian envelope, the fundamental mode in our open-Dirac cavity with hexagonal boundaries has a flat envelope for all cavity sizes. This is confirmed in Fig. 2b for open-Dirac cavities of sizes *D*=19a, *D*=35a, and *D*=51a. Such mode locks all the resonators at the surface of the laser (aperture) in phase regardless of the size of the cavity. The flatness of the envelope means that emission from the edge scales as the perimeter while emission from the surface scales as the area. The scaling of the higher order modes can be understood by extending Eq. (1) for finite systems. Considering the first three modes, the eigenfrequencies for a finite cavity can be obtained by diagonalizing,

$$\begin{pmatrix} -\sigma_k + j\gamma_B & 0 & 0 \\ 0 & -\sigma_k + j\gamma_B & \beta\delta_k \\ 0 & \beta\delta_k & \epsilon + \sigma_k + j\gamma_E \end{pmatrix} \begin{pmatrix} |0\rangle_B \\ |1\rangle_B \\ |2\rangle_E \end{pmatrix} = \mathbf{\Omega}(D) \begin{pmatrix} |0\rangle \\ |1\rangle \\ |2\rangle \end{pmatrix}, \quad (2)$$

where the subscripts B and E on the left-hand side indicate the pure nature of modes and γ_B and γ_E are the loss rates for the B and E modes induced by the boundaries of the cavity. $\mathbf{\Omega}(D)$ is a diagonal matrix with elements representing the complex eigenfrequencies of the finite cavity (see Supplementary Information). Since the dispersion of the B and E bands has an opposite sign, the uncertainty in momentum caused by the finite size will shift the frequencies of the two bands in opposite directions. Thus, σ_k has an opposite sign for the modes originating from the B band than for the modes originating from the E band.

To demonstrate the validity of this model, we computed modes of open-Dirac cavities of different sizes and for holes radii smaller than, equal to, and greater than the critical radius r_{Dirac}. Note that we only present the first three modes of the cavities as modes of higher order have a lower quality factor (Q). The computation was performed using a three-dimensional finite-element solver for the transverse electric polarization that corresponds to the polarization providing the highest gain for the multiple quantum wells used in our work. Figure 3a-c (markers) present the computed frequency shifts of the first three cavity modes. The frequency shifts are computed by comparing cavity modes to the frequency of the B-mode at the Γ-point for an infinite membrane with holes of the same radius. Figure 3d-f (markers) show the scaling of the Q-factor of the same three modes with increasing cavity sizes. The solid lines are obtained by fitting the simulation data with Eq. (2). When the radius of holes is not close to r_{Dirac}, cavity mode $|1\rangle$ asymptotes to the frequency of the fundamental mode at a rate of D^{-2}. This is shown in Fig. 3g along with the scaling for r_{Dirac} in which case the separation increases and scales at the rate of D^{-1}. Note that cavity mode $|1\rangle$ flips from being at a lower frequency than the fundamental mode for $r < r_{\mathrm{Dirac}}$ to a greater frequency than the fundamental mode for $r > r_{\mathrm{Dirac}}$. We also observe that even for the cavity with linear dispersion, the frequency separation rapidly drops to about a terahertz when the diameter of the aperture reaches D=31a (see Supplementary Information). The gain spectrum of semiconductors and notably the quantum wells on which the devices were fabricated, spans almost 100 THz which is much larger than real mode spacing. The selectivity of the lasing mode can thus not be enabled by the scaling of the frequency shift afforded by linear dispersion alone as initially claimed [21-23].

We now investigate the quality factor (Q) of our proposed open-Dirac cavities, with a hexagonal truncation. As previously discussed, the truncation of the cavity serves as selector of the fundamental mode $|0\rangle$ shown by circles on solid lines in Fig. 3. Cavity mode $|1\rangle$ and cavity mode $|2\rangle$ are denoted by square and triangle markers in Fig. 3a-f. Figure 3d-f (markers) show that, as expected, the Q-factor of all the modes increases with the size. We also observe that the Q-factor of the fundamental mode (Q_0) decreases as the radius of the air-holes increases. This can be attributed to a decrease in the average refractive index of the membrane which reduces the confinement of light. Analogous to the scaling of frequency, we observe that the Q-factor of cavity mode $|1\rangle$ asymptotes to Q_0 when r is detuned from r_{Dirac} [see Fig. 3d ($r < r_{\mathrm{Dirac}}$) and Fig. 3f ($r > r_{\mathrm{Dirac}}$)]. Surprisingly, when cavities are tuned to the Dirac point ($r = r_{\mathrm{Dirac}}$) higher-order modes do not asymptote to the fundamental mode anymore as seen in Fig. 3e. They lose energy at a rate always higher than the fundamental mode. Unlike the normalized real-free-spectral range that still decays quickly with the size (Fig. 3g), the normalized imaginary-free-spectral range maintain a non-decaying value despite increasing cavity sizes (Fig. 3h). The loss rates of the modes scale with the size of the cavity as $\gamma_i = c_i D^{-1} + d_i D^{-2}$(see Supplementary Information), where $i = \mathrm{B}$ or E, c_i and d_i are loss rates introduced due to effects of the boundaries. Since the C_6 symmetry of the cavity is more favorable for the B modes, we find that $d_{\mathrm{E}} > d_{\mathrm{B}}$, and $c_{\mathrm{E}} > c_{\mathrm{B}}$.

Moreover, as cavity modes $|1\rangle$ and $|2\rangle$ are formed from an admixture of both B and E modes, when ε→0 their loss rate is dominated by γ_E. Hence, for $D \to \infty$, the normalized complex free-spectral range tends towards a non-vanishing value of $1 - \frac{c_B}{c_E} \sim 0.8$. Theoretical results, plotted in Fig. 3a-h as continuous lines, are in perfect agreement with numerical simulations (markers). The imaginary-free-spectral range in open-Dirac cavities is thus scale invariant. According to the Bloch theorem, cavity modes are the product of the envelopes and unit-cells wavefunctions. The flat envelope fundamental mode (Fig. 2) and the non-vanishing complex free-spectral range (Fig. 3) prevent cavity-scale and unit-cell-scale spatial hole burnings respectively. Mixed higher order modes means that the cross-saturation is comparable to the self-saturation [24]. Single-mode operation is thus guaranteed for scaled up surface emitting lasers operated around open-Dirac singularities (see Supplementary Information).

To experimentally demonstrate our theory, we characterized Berkeley Surface Emitting Lasers (BerkSELs) of diameter *D*=19a (Fig. 4a), *D*=27a (Fig. 4e), *D*=35a (Fig. 4i), *D*=43a (Fig. 4m) and *D*=51a (Fig. 4q). The cavities were optically pumped at room temperature with a pulsed laser (λ = 1,064 nm, T = 12 ns pulse at a repetition rate f = 215 kHz) and the emission from each aperture was collected through a confocal microscope optimized for near-infrared spectroscopy (see Supplementary Information). The signal was directed toward a monochromator coupled to a InGaAs photodiode for spectral measurements. Figure 4 presents the evolution of the normalized output power as a function of the wavelength and the size of the cavity for unit-cell holes radii smaller than the singular radius r_{Dirac} (b, f, j, n, r), equal to r_{Dirac} (c, g, k, o, s), and greater than r_{Dirac} (d, h, l, p, t). For *D*=19a, cavities are single mode for $r < r_{\text{Dirac}}$ (b), $r = r_{\text{Dirac}}$ (c), and $r > r_{\text{Dirac}}$ (d). For *D*=27a, cavities remain single mode for $r < r_{\text{Dirac}}$ (f), $r = r_{\text{Dirac}}$ (g), and $r > r_{\text{Dirac}}$ (h). This is because these cavities are relatively small. However, when the size of cavities is increased to *D*=35a or larger, we observe that they become multimode for $r < r_{\text{Dirac}}$ (j, n, r), remain single mode for $r = r_{\text{Dirac}}$ (k, o, s), and become multimode for $r > r_{\text{Dirac}}$ (l, p, t). The Dirac singularity erases higher-order modes in open-Dirac cavities and BerkSELs remain single-mode when their size is increased. It is worth noting that the uniform field profile across the aperture for the fundamental mode (Fig. 2) and the non-vanishing FSR (Fig. 3) depletes gain across the aperture, making it more difficult for higher-order modes to lase. Single-mode lasing is thus maintained in BerkSELs even for near-damage-threshold pump power. BerkSELs are thus robust to size and pump power density scaling because of the non-vanishing complex free-spectral range and the participation of all unit-cells (or resonators) in the aperture to the lasing mode. These experiments validate our theory and make BerkSELs scale-invariant surface emitting lasers. The apparent high threshold power density of our BerkSELs originates from surface recombination since we are directly structuring the quantum wells, and it is comparable to previously reported lasers using a similar strategy [25]. This can be alleviated by designing alternative structures or by additional chemical treatments of the devices. BerkSELs are in principle infinitely scalable if the proposed open-Dirac potential can be implemented exactly. In practice, considerations such as proximity effects in lithography, electrical injection, or heat release will need to be addressed for high power devices. Assuming typical fabrication imperfections with a variation of hole radii on the order of five nanometers, the fundamental mode is found to be robust to disorder (see Supplementary information).

To further characterize the single-mode lasing of BerkSELs, we present in Fig. 5 the light-light curve (Fig. 5a), the second-order autocorrelation at zero delay $g^2(\tau=0)$ [Fig. 5b] and its pulse width (Fig. 5c). The three different regimes corresponding to spontaneous emission (blue region), amplified spontaneous emission (ASE) [yellow region], and stimulated emission (red region) are observed as the pump power is increased. The second-order autocorrelation function shows a transition from spontaneous emission to amplified spontaneous emission (ASE) as its width drops sharply and the bunching $g^2(0)$ increases. The transition from ASE to stimulated emission is evident from $g^2(0)$ decreasing to unity (Fig. 5b) and the width gradually increasing after the lasing threshold (Fig. 5c), unambiguously proving single-mode lasing action from BerkSELs [26-27]. To confirm that lasing originates from the theoretically predicted B-mode (see Fig. 2 and Fig. 3), experimental far-fields (Fourier space images) of BerkSELs under optical pumping are presented for cavity sizes of D=11a (Fig. 5d), D=19a (Fig. 5e), D=27a (Fig. 5f), D=35a (Fig. 5g), and D=51a (Fig. 4h). The six-fold symmetry of the beams match with the far-field obtained from simulations of finite cavities (see Supplementary Information). The far-fields originate from the B mode with a topological charge of two (see Supplementary Information). Scaling up the cavity size manifests in a smaller beam divergence as expected. We plotted the measured beam divergence as a function of the size of the cavity. The measured beam divergence matches with our theory, and it scales as $1/D$ where D is the diameter of the cavity, in full agreement with theory for modes with a flat envelop fully covering an aperture [28]. It is worth noting that BerkSELs are scalable to large size while bound state in the continuum lasers become multimode when their size is increased, and the latter are more suited for small-scale lasers as previously demonstrated [25]. To the best of our knowledge, there is no known laser or cavity, be it topological, polaritonic, or of any other type, with the scale invariance hereby proposed and demonstrated.

We have thus demonstrated scale-invariant surface emitting lasers that remain single mode when the size of the cavity is increased. They are based on open-Dirac singularities and are robust against size scaling. The unconventional scaling stems from a complex free-spectral range that does not vanish with the size of cavities and the existence of a flat envelope fundamental mode that has never been predicted nor observed in a potential well. Around the open-Dirac singularity, higher-order modes are effectively suppressed by their admixture with more lossy-bands of the structure. The fundamental mode with a flat envelope makes all resonators in the aperture participate in the mode. The fundamental mode thus effectively locks all unit-cells (or resonators) in the aperture in phase, a long-standing challenge. Lasers based on such cavities are surface emitting lasers that we named Berkeley Surface Emitting Lasers (BerkSELs). We have confirmed single-mode lasing from BerkSELs by measuring their second order intensity correlation. We have further confirmed the lasing mode by measuring far-field emissions that agree with our theory. These results demonstrate the fundamental importance of openness and mode admixtures in reciprocal space for enabling scaling in optics, and, they will have implications in linear and non-linear classical and quantum wave-based systems including atoms, electronics, acoustics, phononics, or photonics based on real or synthetic dimensions. The simplicity of BerkSELs makes them universal lasing apertures, readily relevant to applications including virtual reality systems, lidars, interconnects, data centers, manufacturing, defense, or lasers for imaging and medicine.

Figure 1| Scalable open-Dirac electromagnetic cavity and Berkeley Surface Emitting Laser (BerkSEL). a, Top view scanning electron micrograph of a hexagonal lattice photonic crystal (PhC) that is truncated to form an open-Dirac electromagnetic cavity. The free-standing structure is suspended via six bridges connecting the main membrane to the substrate along the ΓK direction. The cavities are fabricated using electron beam lithography, inductively coupled plasma etching, and wet etching (see Supplementary Information). **b,** Tilted view of the cavity showing two bridges, the array of holes, and the PhC-air boundary. The thickness of the membrane is 200 nm, the period of the crystal is 1265 nm, and the radius of holes is used to tune cavities around the Dirac singularity. The inset shows the quality of the nanofabrication with near-perfect circular air-holes interfaces. **c,** Dispersion of the structure displaying a conical degeneracy at 193.5 THz for holes radii of r_{Dirac} = 273 nm. The blue sheet corresponds to the frequency of the B-mode and the red sheets correspond to E modes. The truncation of the crystal, that opens the Dirac cone, is notably chosen to be more favorable for the B-mode compared to the E-modes. The iso-frequency contours, projected on the (k_x, k_y) plane, are sketched together with a representation of laser emission originating from the Dirac point. $\hbar$ is the reduced Planck constant and ω is the angular frequency. The inset presents the Brillouin zone. **d,** Schematic of a Berkeley Surface Emitting Laser (BerkSEL) illustrating the pump beam (blue) and the lasing beam (red) from an unconventional open-Dirac cavity mode that synchronizes all unit-cells (or resonators) in phase. Therefore, all unit-cells in the aperture participate in the lasing mode.

Figure 2| Quantization of the band structure in open-Dirac cavities forming higher-order modes and evidence for an unconventional fundamental mode with a flat envelope. a, Cavity modes on the dispersion of the unit-cell (dashed lines) presented in color to indicate the mixing of the B and E bands. The fundamental mode at the Γ-point is the only purely B mode (cyan). Higher-order modes (copper) are photonic admixtures of the B and E bands and thus demonstrate a different scaling than the fundamental mode. The blur around cavity modes indicates the uncertainty in momentum σ_k due to the finite size of the cavity, and the spacing between the modes is the momentum imparted by the cavity δ_k. The cavity provides greater feedback along the M-direction and linear dispersion causes modes to be equispaced in frequency. The electric field intensity of the five lowest order modes for a cavity of size *D*=51a (where a is the size of the unit-cell) is shown on the right. **b,** Phase of the out-of-plane component of the magnetic field (sampled at the same point in each unit-cell along the diagonal of the cavity) and magnitude of the electric field (averaged over each unit-cell along the diagonal of the cavity) for cavities of sizes *D*=19a, *D*=35a, and *D*=51a. The fundamental mode |0> has an unconventional flat envelope for all cavity sizes. A zoom-in view of the field distribution in unit-cells is presented in Supplementary Information.

Figure 3| Complex frequency scaling of open-Dirac electromagnetic cavities. Frequency shifts of the first three cavity modes for (**a**) $r < r_{\mathrm{Dirac}}$, (**b**) $r = r_{\mathrm{Dirac}}$, (**c**) $r > r_{\mathrm{Dirac}}$, computed by comparing cavity modes to the frequency of the B-mode at the Γ-point for an infinite membrane with holes of the same radius. Quality factor of the first three cavity modes for (**d**) $r < r_{\mathrm{Dirac}}$, (**e**) $r = r_{\mathrm{Dirac}}$, (**f**) $r > r_{\mathrm{Dirac}}$. **g,** Scaling of the frequency for various radii. When r is detuned from r_{Dirac}, the dispersion is quadratic, and the frequency shift scales as D^{-2}. When r is tuned to r_{Dirac} the frequency shift scales as D^{-1}. **h,** Scaling of the quality factor when the radius is detuned from r_{Dirac} and when it is tuned to the singularity. For quadratic dispersion, cavities have an imaginary free-spectral range that vanishes with the size of cavities. Very interestingly, the normalized imaginary free-spectral range does not vanish with the size for our open-Dirac cavities that can thus be scaled up in size. For all plots (a-h), markers are numerical simulations and continuous lines are theory based on our model.

Figure 4| Lasing characteristics of BerkSELs erasing higher-order modes around the open-Dirac singularity. Top-view SEM of fabricated open-Dirac cavities of size *D*=19a (**a**), *D*=27a (**e**), *D*=35a (**i**), *D*=43a (**m**), and *D*=51a (**q**), where *D* is the diameter of the aperture and a is the size of the unit-cell of the photonic crystal. The scale bars represent 25µm. Evolution of the normalized output power as a function of the wavelength and the size of the cavity for unit-cell holes radii smaller than the singular radius r_{Dirac} (**b**, **f**, **j, n, r**), equal to r_{Dirac} (**c**, **g**, **k, o, s**), and greater than r_{Dirac} (**d**, **h**, **l, p, t**). The pump power density is 1.1µW/µm^2 in all cases. For *D*=19a, cavities are single mode for $r < r_{Dirac}$ (**b**), $r = r_{Dirac}$ (**c**), and $r > r_{Dirac}$ (**d**). For *D*=27a, cavities are single mode for $r < r_{Dirac}$ (**f**), $r = r_{Dirac}$ (**g**), and $r > r_{Dirac}$ (**h**). When the size is increased to *D*=35a, *D*=43a, and *D*=51a, we observe that cavities become multimode mode for $r < r_{Dirac}$ (**j, n, r**), remain single mode for $r = r_{Dirac}$ (**k, o, s**), and become multimode again for $r > r_{Dirac}$ (**l, p, t**). The Dirac singularity erases higher-order modes in open-Dirac cavities and BerkSELs remain single-mode when the size is increased. These experiments validate our theory and make BerkSELs scale-invariant surface emitting lasers.

Figure 5| Far-field scaling of BerkSELs and photon statistics. a, Emitted output power of a BerkSEL of aperture diameter *D*=35a (where a is the size of the unit-cell) as a function of the average pump power density (light-light curve). **b, c,** Second order intensity autocorrelation measurements at zero delay $g^2(0)$ (**b**) and its pulse width (**c**). The pulse width of the second-order autocorrelation function shows a distinct transition from spontaneous emission to amplified spontaneous emission (ASE) as the width drops sharply and then from ASE to stimulated emission as the width gradually increases. These transitions unambiguously demonstrate single-mode lasing from BerkSELs. Experimental far-fields (Fourier space images) of BerkSELs under optical pumping are presented for cavity sizes of *D*=11a (**d**), *D*=19a (**e**), *D*=27a (**f**), *D*=35a (**g**), and *D*=51a (**h**). The scale bars indicate 10°. Measured and theoretical beam divergence angle as a function of the cavity size. The continuous line is the theoretical prediction and points are experimental data. A good agreement is observed between theory and experiments. The inset shows the same data plotted in log-log scale, demonstrating the 1/*D* scaling of the beam divergence where *D* is the diameter of the aperture (see Supplementary Information). This scaling corresponds to the theoretical limit obtained for modes with a flat envelop fully covering an aperture (see Fig. 2). Error bars indicate the standard deviation of the beam divergence.

Data availability

The data that support the plots within this paper and other findings of this study are available from the corresponding author upon reasonable request.

Code availability

The computer codes that support the plots within this paper and other findings of this study are available from the corresponding author upon reasonable request.

Author contribution

B.K. conceived the project, proposed the idea, and guided the theoretical and experimental investigations. R.C. performed the theoretical calculations. W.N. fabricated the devices. W.R. performed the measurements. W.Q., E.M., S.D., and A.S. contributed to the fabrication of larger size devices requested by the reviewers. All authors contributed to discussions and B.K. wrote the manuscript with input from R.C. and W.R.

Acknowledgements

This research was mostly supported by the Office of Naval Research (ONR) Young Investigator Award (N00014-19-1-2737), the ONR JTO MRI Award (N00014-20-1-2752), the ONR grant N00014-20-1-2723, and the National Science Foundation (NSF) Career Award (ECCS-1929659). It was partially supported by the Laboratory Directed Research and Development Program of Lawrence Berkeley National Laboratory (LBNL) under US Department of Energy contract no. DE-AC02-05CH11231, the NSF QLCI programme through grant number OMA-2016245, the Moore Inventor Fellows program, and the Bakar Fellowship at UC Berkeley. The work was partially performed at the UC Berkeley Marvel Nanofabrication Laboratory, the Molecular Foundry at LBNL, and the San Diego Nanotechnology Infrastructure, a member of the National Nanotechnology Coordinated Infrastructure, which is supported by the National Science Foundation (ECCS-1542148). We thank M. Montero for technical assistance regarding fabrication.

Competing interests

The Regents of the University of California have filed a patent application (US Prov App 63/304,581) on technology related to the processes described in this article.

References:

1. Schawlow, A. L. & Townes, C. H. Infrared and Optical Masers. *Phys. Rev*. **112**, 1940–1949 (1958).
2. Kogelnik, H. & Shank, C. V. Stimulated emission in a periodic structure. *Appl. Phys. Lett*. **18**, 152–154 (1971).
3. Soda, H., Iga, K., Kitahara, C. & Suematsu, Y. GaInAsP/InP Surface Emitting Injection Lasers. *Jpn. J. Appl. Phys*. **18**, 2329 (1979).
4. Meier, M. et al. Laser action from two-dimensional distributed feedback in photonic crystals. *Appl. Phys. Lett*. 74, 7-9 (1999).
5. Imada, M. et al. Coherent two-dimensional lasing action in surface-emitting laser with triangular-lattice photonic crystal structure. *Appl. Phys. Lett*. **75**, 316–318 (1999).
6. Choquette, K. D., Hou, H. Q., Geib, K. M. and Hammons, B. E,: “Uniform and high power selectively oxidized 8x8 VCSEL array”. 1997 Dig. *IEEE/LEOS Summer Topical Meetings*, Montreal, Quebec, Canada, 11–15 August 1997, pp. 11–12
7. D. Francis, H.-L. Chen, W. Yuen, G. Li, and C. Chang-Hasnain, “Monolithic 2D-VCSEL array with 2 W CW and 5 W pulsed output power,” *Electron Lett*., vol. **34**, pp. 2132–2133, 1998.
8. M. Yoshida *et al.*, “Double-lattice photonic-crystal resonators enabling high-brightness semiconductor lasers with symmetric narrow-divergence beams” *Nature Materials* **18**, 121–128 (2019).
9. Novoselov, K. S. et al. Electric field effect in atomically thin carbon films. *Science* **306**, 666–669 (2004).
10. Haldane, F. D. M. Model for a quantum Hall effect without Landau levels: condensed-matter realization of the “parity anomaly”. *Phys. Rev. Lett*. **61**, 2015–2018 (1988).
11. Yablonovitch, E. Inhibited Spontaneous Emission in Solid-State Physics and Electronics. *Phys. Rev. Lett*. **58**, 2059–2062 (1987).
12. John, S. Strong localization of photons in certain disordered dielectric superlattices. *Phys. Rev. Lett*. **58**, 2486–2489 (1987).
13. Sakoda, K. Universality of mode symmetries in creating photonic Dirac cones. *J. Opt. Soc. Am*. B **29**, 2770 (2012).
14. Sakoda, K. Proof of the universality of mode symmetries in creating photonic Dirac cones. *Opt. Express* 20, 25181 (2012).
15. Enoch, S., Tayeb, G., Sabouroux, P., Guérin, N. & Vincent, P. A Metamaterial for Directive Emission. *Phys. Rev. Lett*. **89**, 213902 (2002).
16. Huang, X., Lai, Y., Hang, Z. H., Zheng, H. & Chan, C. T. Dirac cones induced by accidental degeneracy in photonic crystals and zero-refractive-index materials. *Nature Materials* **10**, 582–586 (2011).
17. Moitra, P. *et al.*, Realization of an all-dielectric zero-index optical metamaterial. *Nature Photonics* **7**, 791–795 (2013).
18. Li, Y. *et al.*, On-chip zero-index metamaterials. *Nature Photon*. **9**, 738–742 (2015).
19. Liberal, I. & Engheta, N. Near-zero refractive index photonics. *Nature Photon*. **11**, 149–158 (2017).
20. Jacqmin, T. *et al.* Direct observation of Dirac cones and a flatband in a honeycomb lattice for polaritons. *Phys. Rev. Lett*. **112**, 116402 (2014).

21. Bravo-Abad, J., Joannopoulos, J. D. & Soljacic, M. Enabling single-mode behavior over large areas with photonic Dirac cones. *Proc. Natl Acad. Sci. USA* **109**, 9761–9765 (2012).
22. Chua, S.-L., Lu, L., Bravo-Abad, J., Joannopoulos, J. D. & Soljačić, M. Larger-area single-mode photonic crystal surface-emitting lasers enabled by an accidental Dirac point. *Opt. Lett*. **39**, 2072 (2014).
23. Gao, X. et al. Dirac-vortex topological cavities. Nature Nanotechnology **15**, 1012–1018 (2020).
24. Siegman, A. E. Lasers 466-472 (University Science Book, 1986).
25. Kodigala, A. et al. Lasing action from photonic bound states in continuum. Nature **541**, 196–199 (2017).
26. Loudon, R. The Quantum Theory of Light 3rd edn (Oxford Univ. Press, 2000).
27. Pan, S. H., Gu, Q., El Amili, A., Vallini, F. & Fainman, Y. Dynamic hysteresis in a coherent high-β nanolaser. *Optica* **3**, 1260-1265 (2016).
28. The Regents of the University of California filed a patent on systems, methods, and applications using principles described in this paper to control lasers and open-wave systems.

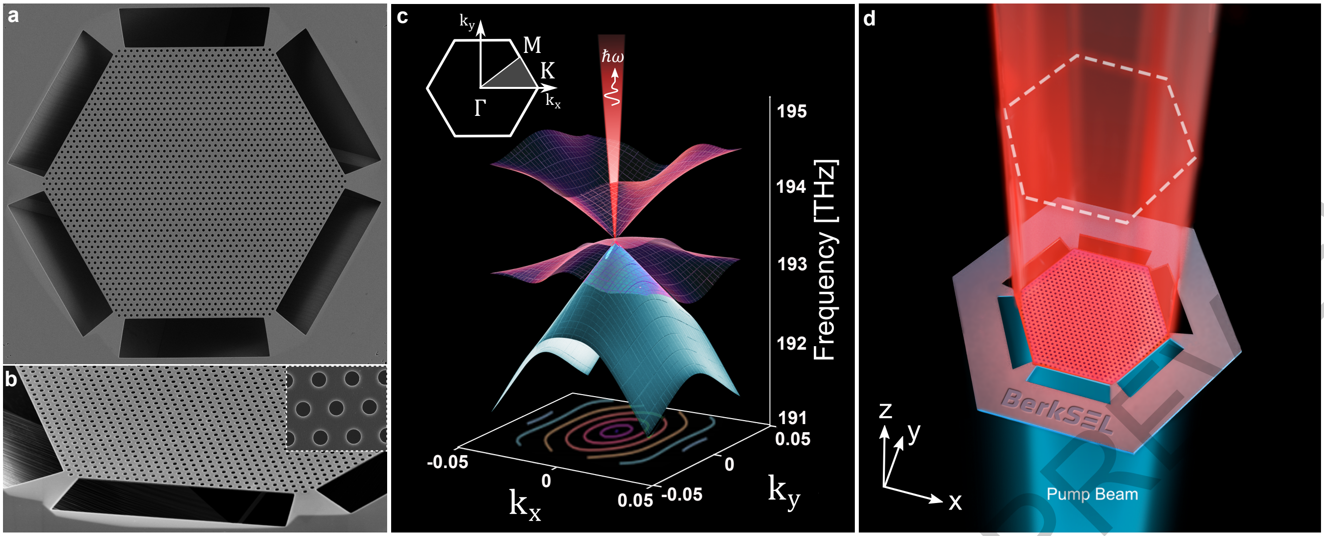
a
b
c
k_y
M
K
k_x
Γ
$\hbar\omega$
195
194
193
192
191
Frequency [THz]
-0.05
0
0.05
k_x
-0.05
0
0.05
k_y
d
z
y
x
BerkSEL
Pump Beam

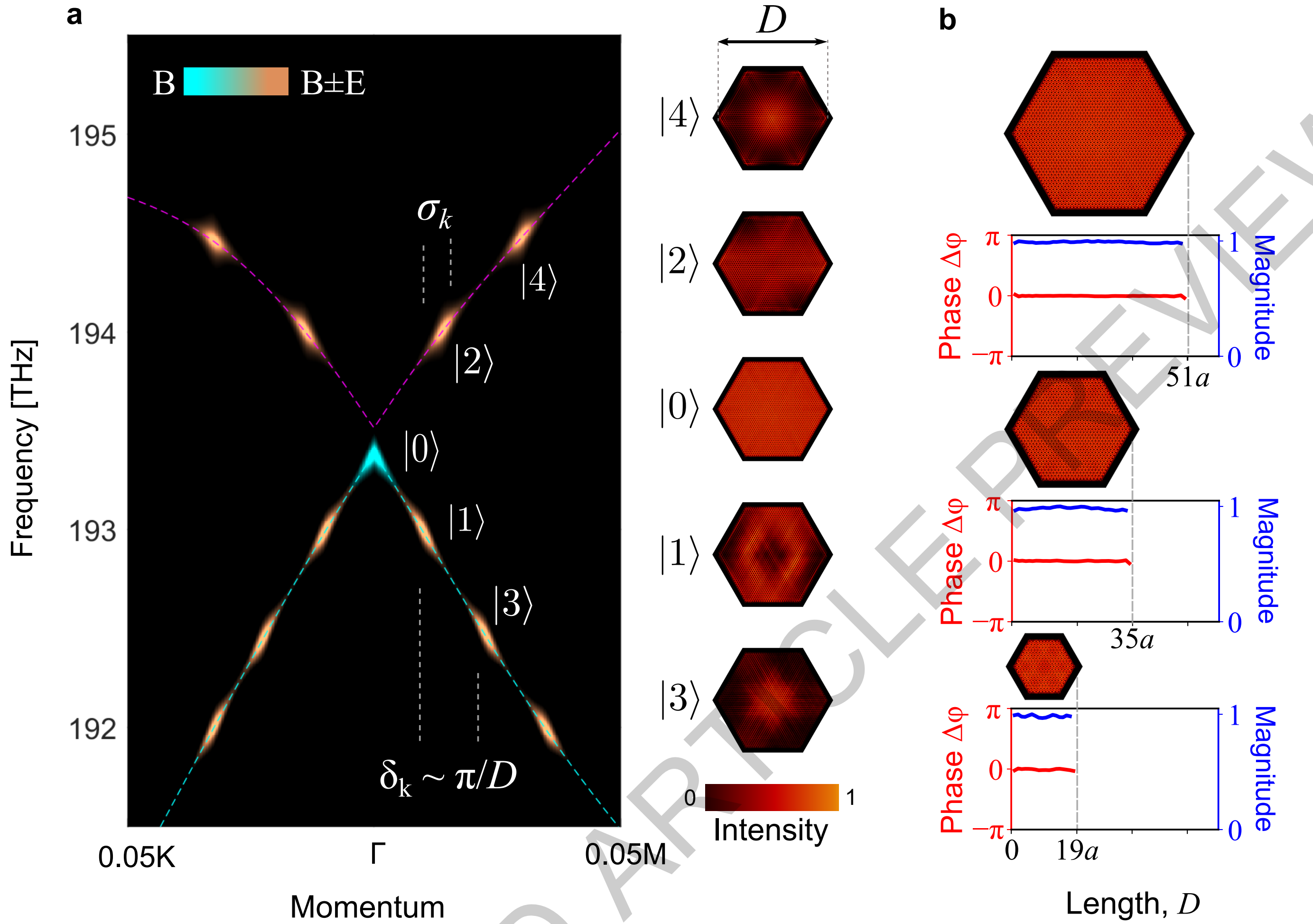

a
B
B±E
195
194
193
192
Frequency [THz]
σ_k
$|4\rangle$
$|2\rangle$
$|0\rangle$
$|1\rangle$
$|3\rangle$
$\delta_k \sim \pi/D$
0.05K
Γ
0.05M
Momentum
D
0
1
Intensity
b
Phase Δφ
Magnitude
π
0
−π
1
0
51a
35a
19a
Length, D

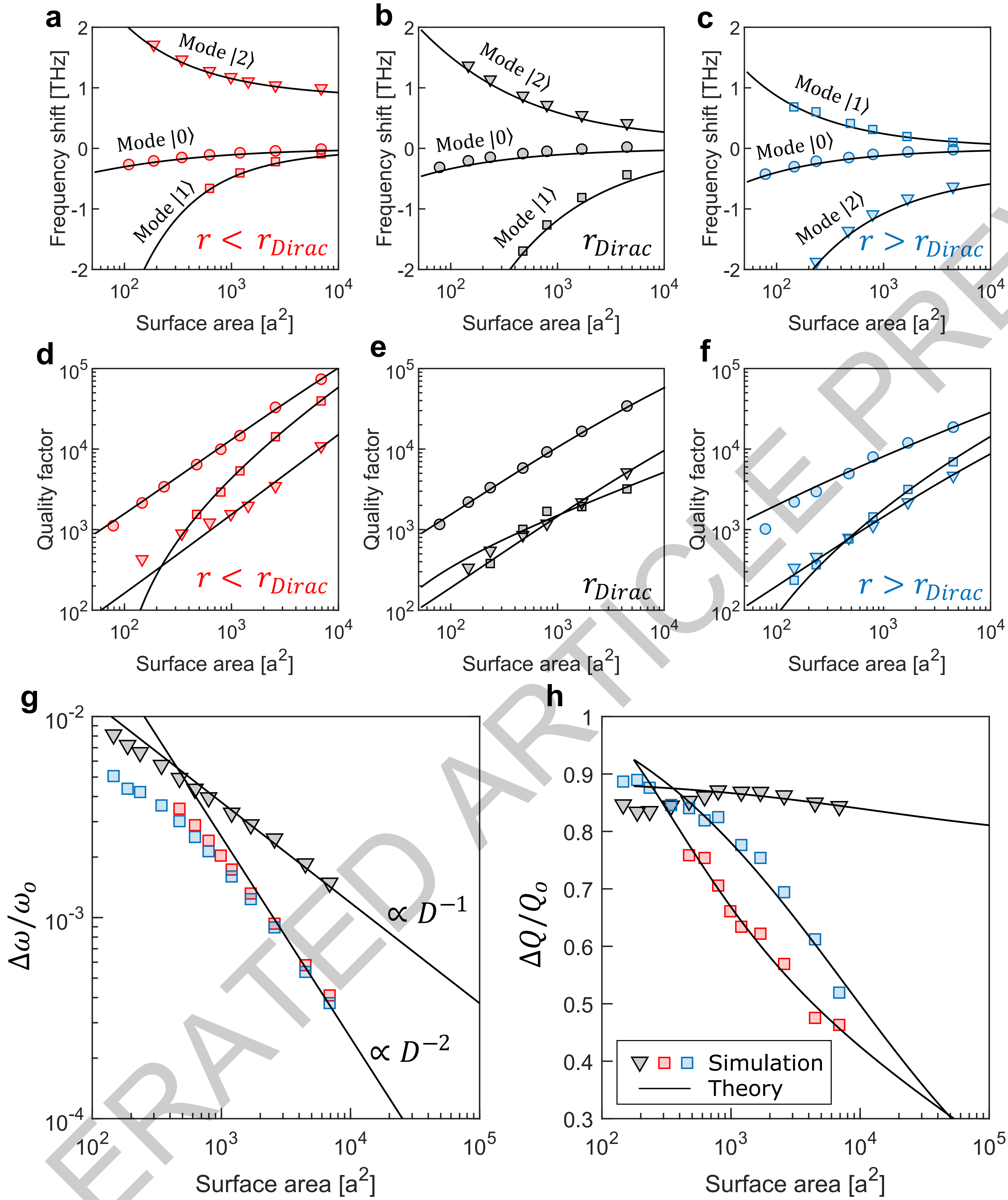
a
b
c
Mode |2⟩
Mode |0⟩
Mode |1⟩
Frequency shift [THz]
Surface area [a^2]
r < r_Dirac
r_Dirac
r > r_Dirac
d
e
f
Quality factor
g
Δω/ω_o
∝ D^−1
∝ D^−2
h
ΔQ/Q_o
Simulation
Theory

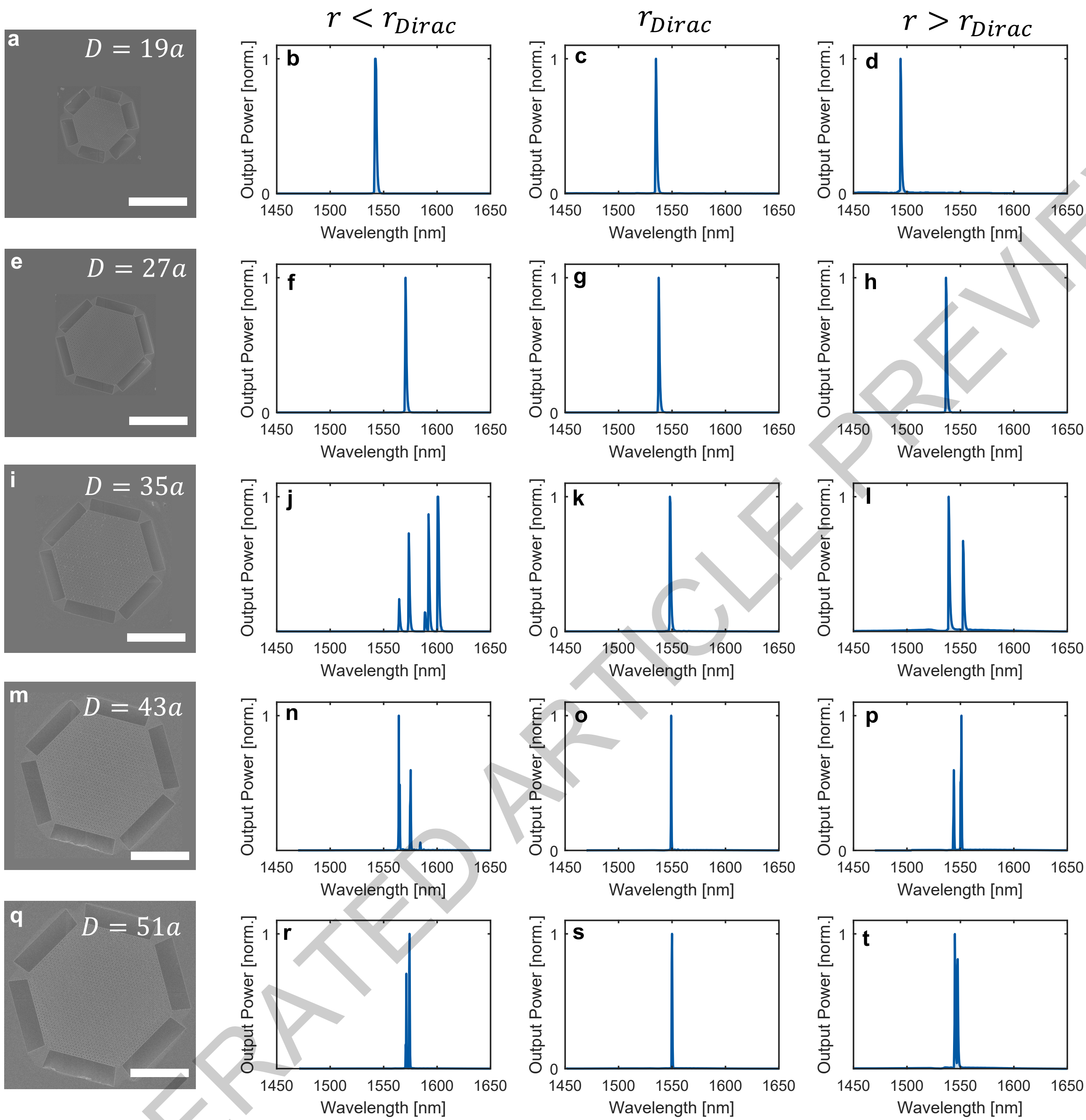

$r < r_{Dirac}$
r_{Dirac}
$r > r_{Dirac}$
a
$D = 19a$
e
$D = 27a$
i
$D = 35a$
m
$D = 43a$
q
$D = 51a$
b
c
d
f
g
h
j
k
l
n
o
p
r
s
t
Output Power [norm.]
Wavelength [nm]
1450
1500
1550
1600
1650
0
1

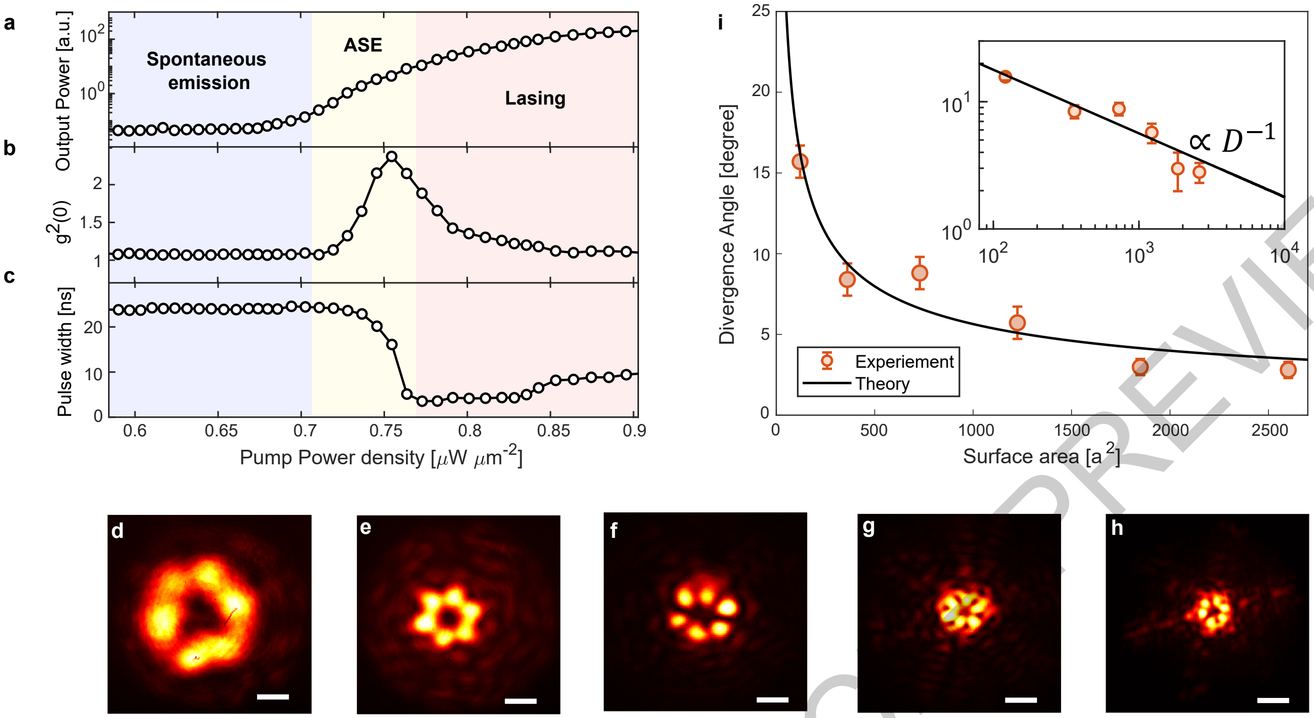

a
b
c
Output Power [a.u.]
Spontaneous emission
ASE
Lasing
$g^2(0)$
Pulse width [ns]
Pump Power density [μW μm^{-2}]
i
Divergence Angle [degree]
Surface area [a^2]
$\propto D^{-1}$
Experiement
Theory
d
e
f
g
h